Sains Malaysiana 45(7)(2016): 1155–1167

Lead Adsorption Behaviours on Nanoscale Zero Valent Irons (nZVI) Coupled with Rice Husk MCM-41

(Kelakuan Penjerapan Plumbum ke atas Besi Bervalensi Sifar pada Skala Nano (nZVI) Berganding dengan Sekam Padi MCM-41)

C. KAEWBUDDEE, P. CHANPIWAT, P. KIDKHUNTHOD & K. WANTALA*

ABSTRACT

The aims of this work were to investigate the characteristics of nanoscale zero valent irons (nZVI) coupled with mesoporous materials (RH-MCM-41) adsorbent and to study the removal mechanisms of Pb (II) from synthetical solutions using full pictorial design batch experiments. Synthetic nZVI coupled with RH MCM-41 as Pb (II) adsorbent were characterized by XRD, TEM, BET and XANES. The results of XANES analyses confirmed the ability of RH-MCM-41 to prevent oxidations of Fe^0 to Fe^{2+} and Fe^{3+}. XANES results also verified the oxidation states of Pb (II). The solution pH was the most significant positive effect in controlling Pb (II) adsorption. The equilibrium and kinetic adsorption isotherms well fitted with the Langmuir isotherm. The pseudo-second order kinetic adsorption indicated that the adsorption process is the rate limiting step for Pb (II) removal. Furthermore, Langmuir-Hinshelwood confirmed the obvious Pb (II) adsorption at the active site of adsorbents. The reduction rate constant (k_r = 5,000 mg/L.min) was higher than the adsorption rate constant (K_{ad} = 0.0002 L/mg). Regarding the research results, four pathways including: reduction process, adsorption on FeOOH, adsorption on RH-MCM-41 and complex reaction between Fe and Pb ions were suggested for Pb (II) removal by nZVI coupled with RH-MCM-41.

Keywords: Adsorption mechanism; mesoporous material; nanoscale zero valent irons; Pb; XANES

ABSTRAK

Penyelidikan ini bertujuan untuk mengkaji ciri besi bervalensi sifar pada skala nano (nZVI) berganding dengan penjerap bahan mesoporous (RH-MCM-41) dan mengkaji mekanisme penyingkiran Pb (II) daripada larutan sistetik menggunakan uji kaji reka bentuk kelompok gambar penuh. Gabungan penjerap sintetik nZVI dengan RH MCM-41 sebagai Pb (II) telah dicirikan oleh XRD, TEM, BET dan XANES. Keputusan analisis XANES mengesahkan keupayaan RH-MCM-41 untuk mengelakkan pengoksidaan Fe^0 kepada Fe^{2+} dan Fe^{3+}. Keputusan XANES ini juga mengesahkan keadaan pengoksidaan Pb (II). Larutan PH adalah kesan positif yang paling penting dalam mengawal penjerapan Pb (II). Penjerapan isoterma keseimbangan dan kinetik juga sepadan dengan isoterma Langmuir. Penjerapan kinetik tertib pseudo-kedua menunjukkan bahawa proses penjerapan adalah langkah untuk mengehadkan kadar penyingkiran Pb (II). Tambahan pula, Langmuir-Hinshelwood mengesahkan penjerapan pasti Pb (II) di tapak bahan penjerap aktif. Kadar pengurangan berterusan (k_r = 5000 mg/L.min) adalah lebih tinggi daripada kadar penjerapan pemalar (K_{ad} = 0.0002 L/mg). Mengenai hasil penyelidikan, empat laluan termasuk: proses pengurangan, penjerapan pada FeOOH, penjerapan pada RH-MCM-41 dan tindak balas kompleks antara ion Fe dan Pb dicadangkan untuk penyingkiran Pb (II) oleh nZVI berganding dengan RH-MCM-41.

Kata kunci: Bahan mesoporos; besi bervalensi sifar pada skala nano; mekanisme penjerapan; Pb; XANES

INTRODUCTION

Concern of lead (Pb) contamination in the environment has been raised in the past few decades due to its high toxicity at very low exposure levels. In the environment, Pb is toxic to plants, animals and microorganisms. For public health, once exposed, Pb can cause acute and chronic effects. Even though natural processes release some amounts of Pb into the environment, human activities are one of the most significant sources of Pb contamination in the atmospheric, aquatic and terrestrial environments. For example, untreated wastewater in southeast Nigeria was found to be contaminated with 15 mg/L of Pb, which was about 2.7 to 75 times higher than concentrations of other heavy metals such as boron, cadmium, copper, iron, manganese, nickel and zinc (Onweremadu 2008).

In nature, Pb is rarely found in its elemental state; however, it is generally present in its ion forms such as monovalent, divalent and tetravalent states. Of all ions present, Pb (II) ions are the most common. Pb (II), one of the toxic inorganic pollutants to aquatic systems, can be released from several industries, including batteries, paints and lead wire production (case studies in Environmental Medicine (CSEM): Lead Toxicity 2010). Pb (II) can be accumulated, once exposed, in a variety of body systems. High blood levels of Pb have been reported by several groups of researchers across the globe, including those in

China, Jamaica, Mexico, Nicaragua, Senegal, Trinidad and Vietnam. For China, Pb levels in blood were found to be as high as 0.8 mg/L (Occupational Knowledge International 2010). These levels were about 8 and 16 folds greater than the standard elevated blood Pb level for adults (0.1 mg/L) and children (0.05 mg/L), respectively (Centers for Disease Control and Prevention 2005). Pb affects multiple body systems such as nervous, reproductive, blood, digestive and urinary (ATSDR - Toxicological Profile 2007). Due to its high toxicity, several environmental protection organizations have set limits of Pb (II) concentration in drinking water, for example, WHO (0.005 mg $L^{-1)}$ and US EPA (0.015 mg/L) (case studies in Environmental Medicine (CSEM): Lead Toxicity 2010, WHO|WHO Guidelines for drinking-water quality 2011). In Thailand, the Pollution Control Department (PCD) is regulating 0.05 mg/L as the standard of Pb in groundwater (notification of the Ministry of Industry Thailand, NO 12, B.E. 2542. 1999).

In order to reduce the potential exposure of Pb (II) in aquatic systems, particularly industrial wastewater, several conventional treatment methods have been introduced, for example, ion exchange, filtration, chemical precipitation and reverse osmosis. However, those methods were relatively expensive and require special attention. Therefore, the adsorption technique, a simpler and cost effective treatment alternative, has been introduced to remove Pb (II) from aqueous systems. Low cost and locally available adsorbents with high removal capacity such as zeolites, chitosan, clay, peat, moss, fly ash, coal, natural oxide, red mud, activated carbon and industrial waste were used to remove Pb (II) in several studies (Babel & Kurniawan 2003; Bhatnagar et al. 2011). Wide ranges of removal efficiencies of 12.32, 113.5, 209.8 and 138.9 mg/g were determined when chitosan-coated sand, orange peel, modified orange peel and valonia tannin resin, respectively, were used as Pb (II) adsorbents. However, the significant drawback of this adsorption technique is a long equilibrium time, up to 120 min (Feng et al. 2004; Şengil & Özacar 2009; Wan et al. 2010). Therefore, small size adsorbent with high surface area and reactivity such as nanoscale zero valent irons (nZVI) (Zhang 2003) was introduced for a rapid removal of several pollutant ions, including Cd (II), Cr (VI), Hg (II), Zn (II) and nitrate (II) (Ahn et al. 2008; Boparai et al. 2013; Hwang et al. 2011; Kržišnik et al. 2014; Ponder et al. 2000; Yan et al. 2010; Zhang et al. 2014). Although nZVI is an effective choice for heavy metal adsorption, its short longevity is the main disadvantage. nZVI should be immediately used after synthesized; otherwise, it will be rapidly oxidized and its surface will be covered by Fe (II) and Fe (III) (Tanboonchuy et al. 2011). Another disadvantage of nZVI is its lack of durability, mechanical strength and tendency of aggregation formation (Kim et al. 2013; Zhang et al. 2010, 2011). Recently, the application of nZVI coupled with a supporting material such as amorphous silica, silica sand and kaolin was developed to enhance efficiency and reduce equilibrium time of metal ions removal. It was found that the efficiency of metal ions removal, especially Pb (II), depends on the surface and elemental compositions of the nZVI supporting materials. In addition, the percentage removal of more than 96% of Pb (II) was observed within 30 min by nZVI supporting materials (Oh et al. 2007; Pojananukij et al. 2016).

In this present study, nZVI coupled with MCM-41 mesoporous material adsorbent was used to remove Pb (II) from aqueous solution. The objectives were to examine the characteristics of nZVI coupled with MCM-41 adsorbent, study the effects of initial pH, adsorption time and types of adsorbents (nZVI with and without MCM-41) on Pb (II) removal efficiency and study the Pb (II) removal mechanism using equilibrium and kinetic isotherms.

Materials and Methods

Experimental Design

Batch experiments were conducted according to the full factorial design (FFD). The experiments contain all possible combinations of a set of three variables as summarized in Table 1.

Chemicals and Reagents

All chemicals used in this study were laboratory grade. Stock solutions containing 250, 300, 350, 400, 450 and 500 ppm of Pb (II) were prepared from $Pb(NO_3)_2$. The total volume of Pb (II) solution of 250 mL was used for each batch experiment. For sample collection, about 10% of a total volume of solution was collected. All experiments were conducted in duplicate.

Rice Husk Silica Extraction and RH-MCM-41 Synthesis

The extraction of rice husk (RH) silica and synthesis of RH-MCM-41 were conducted following the methods developed by Wantala et al. (2012a, 2010). In short, RH was first washed several times with water and dried in an oven at 105°C overnight. Then, it was refluxed in 6 M HCl at 70°C for 5 h. After that, it was rinsed repeatedly with deionized water until neural pH was obtained and dried in an oven at 105°C overnight. Lastly, it was calcined in a muffle furnace at 550°C for 6 h to finally produce the white RH silica.

For the synthesis of RH-MCM-41, the hydrothermal method described by Wantala et al. (2010) was used. Briefly, about 9 g of hexadecyltrimethyl ammonium bromide (CTAB) was dissolved in 180 mL of deionized water and stirred until the solution was well mixed. Meanwhile, sodium silicate solution was prepared by mixing 12 g of NaOH and 60 mL of deionized water. Then, 6 g of RH silica was added to sodium silicate solution. After that, CTAB solution was dropped into sodium silicate solution. The mixture was stirred and adjusted to pH of 11. Afterward, the solution was placed in an autoclave at 100°C for 72 h. After the hydrothermal process, the

suspended solid was filtered through Whatman filter paper and washed by deionized water until the pH was about 7. Lastly, it was dried in an oven at 100ºC and calcined in the muffle furnace at 550ºC for 6 h.

PREPARATION OF nZVI

nZVI was synthesized using a nanoscale reduction process described elsewhere (Krasae et al. 2014; Tanboonchuy et al. 2011). In order to summarize, 0.045 M of ferric ion (Fe^{3+}) was reduced into zero valent iron (Fe^0) by using 0.25 M sodium borohydride ($NaBH_4$), as shown in Reaction 1. With vigorous mixing condition, sodium borohydride was slowly dropped into ferric chloride, and washed with deionized water for 3 times. After that, nZVI was separated using a magnet and immediately used in the batch experiments.

$$Fe(H_2O)_6^{3+}+3BH_4^-+3H_2O \rightarrow Fe^0+3B(OH)_3+10.5H_2O \quad \text{(Reaction 1)}$$

PREPARATION OF NZVI COUPLED WITH RH-MCM-41

Preparation of nZVI coupled with RH-MCM-41 can be separated into 2 steps; nZVI preparation and nZVI coupled with RH-MCM-41 preparation. First, nZVI was prepared following the nanoscale reduction method described previously (Reaction 1). Second, about 2 g RH-MCM-41 was mixed with 0.4 g of nZVI in an aqueous solution. After that, nZVI coupled with RH-MCM-41 was separated using a magnet and immediately used in the batch experiments.

ADSORBENT CHARACERIZATIONS

Phase and crystallinity of nZVI and RH-MCM-41 were determined using the X-ray diffractometer with CuKα at 0.1514 nm wavelength at 40 mA and 40kV (Model D8 Discover, Bruker AXS, Germany). The morphologies of nZVI, RH-MCM-41 and nZVI coupled wih RH-MCM-41 were investigated using the transmission electron microscope (TEM, TECNAI G^2 20S – TWIN, FEI, Czech Republic). The specific surface area of all adsorbents was measured and calculated using the N_2-sorption isotherm and the Brunauer-Emmett-Teller (BET) method (ASAP 2010, Micromeritics, USA), respectively.

The oxidation states and oxidative species of Fe in adsorbents were determined by the X-ray absorption near edge structure (XANES) technique at the beamline-2.2 of the Synchrotron Light Research Institute (SLRI: Public Organization). XANES measurements were simultaneously recorded at Fe K-edge (7112 eV) in the transmission mode for 10 s within 30 min of adsorption times. The Fe foil, FeO and Fe_2O_3 were used as standard references. Meanwhile, the oxidation states and oxidative species of Pb in both nZVI and nZVI coupled with RH-MCM-41 obtained from the complete adsorption process were determined by the XANES technique at the beamline-5.2 of the SLRI. The measurements were simultaneously recorded at Pb M-edge (2,484 eV) in the transmission mode. The Pb foil and PbO were used as standard references. The data reduction, including background removal and normalization, were performed using the Athena program.

ADSORPTION EXPERIMENT

Adsorption experiments concerning factors affecting Pb (II) removal efficiency (Table 1) were conducted. The initial concentration of Pb was 500 ppm. The volume of solution used was 250 mL. The adsorbent loading per lier of solution was 0.4 g of nZVI and 2 g of RH-MCM-41 (RH-MCM-41/nZVI mass ratio = 5). Pb concentrations in solution were analyzed by the flame atomic absorption spectrophotometer (FAAS) (Perkin Elmer, 100AAnalyst, USA). Removal efficiency of Pb (II) of each experiment was calculated using (1).

$$Y(\%) = \frac{C_0 - C_t}{C_0} \times 100, \quad (1)$$

where Y is percentage of Pb (II) removal; C_0 is initial Pb (II) concentration (ppm); and C_t is Pb (II) concentration (ppm) after adsorption experiment (min).

STUDY OF PB (II) REMOVAL MECHANISM

RH-MCM-41/nZVI mass ratio of 5 was used for the equilibrium and kinetic study. The initial Pb (II) concentrations varying from 250 to 500 ppm in 250 mL batch experiment were used. The adsorbent loading was 0.6 g. The solution pH was maintained at 6. The equilibrium adsorption isotherms were examined using Langmuir and Freundlich isotherms. The Temkin and Dubinin-Radushkevich isotherms was used to determine sorption energies. The kinetic adsorption isotherms were calculated using the pseudo-first order, pseudo-second order, intrapaticle diffusion and Langmuir-Hinshelwood (LH).

TABLE 1. Detailed experimental design with all factors affecting to Pb (II) removal efficiency

Variables	Levels		
	Low (-1)	Medium (0)	High (+1)
Adsorbents; (X_1)	nZVI	-	nZVI coupled with RH-MCM-41
Initial pH; (X_2)	3	4.5	6
Adsorption time (min); (X_3)	3	5	7

Results and Discussion

Adsorbent characteristics and morphologies

The crystallinity of nZVI, RH-MCM-41 and nZVI coupled with RH-MCM-41 was examined by X-ray diffractograms, using CuK radiation in an angular (2θ) from 20 to 70 with 40 mA and 40 kV. Figure 1(a) shows the angular XRD pattern of RH-MCM-41 with an angle (2θ) from 0 to 15. The reflection of silicon dioxide crystals found at 2 was 2.3, 3.1, 4.5 and 5.9 and correspond to the reflection plane of 100, 110, 200 and 210, respectively. These signals clearly indicate the long-rang orders of hexagonal mesoporous structure, which is the main characteristic of MCM-41 reported by Melo et al. (1999), Wantala et al. (2012b) and Zhang et al. 2013. The appearance of the peak 2θ at 45° (Figure 1(b)) confirmed that the zero valent iron (Fe^0) was predominantly presented in nZVI. However, as shown in Figure 1(b), the crystallinity of nZVI in the nZVI coupled with RH-MCM-41 could not be observed at 45° (2θ).

Figure 2 shows the results of TEM analyses of all adsorbents. The hexagonal array or honey-comb structure of RH-MCM-41 is depicted in Figure 2(a). While, Figure 2(b) clearly confirmed that nZVI particles consist of a specific core-shell structure, an inner core of zero valent iron and a thin shell of iron oxide, FeOOH. The morphology of nZVI found in this present study was in good agreement with results of the nZVI core-shell structure reported by many researchers (Liang et al. 2014; Li & Zhang 2007; Sun et al. 2006; Yan et al. 2010; Zhang et al. 2013).

As clearly displayed in Figure 3(a) and 3(b), both nZVI and nZVI coupled with RH-MCM-41 exhibit a slight change in oxidation state of Fe from 0 to higher oxidation states (2+ and 3+). This change in oxidiation state can be confirmed by a slight shift in edge energy of samples. However, it was found that the change in oxidation state of nZVI was more rapid than of nZVI coupled with RH-MCM-41, as indicated by the shoulder and white line in Figures 3(a) and 3(b). The pre-edge peak energies of oxidation state of Pb (II) in both nZVI and nZVI coupled with RH-MCM-41 after adsorption process lie between Pb^0 and Pb^{2+} (Figure 4). Thus, it can be implied that there is a combination of Pb ions (0 and 2+ oxidation).

Adsorption efficency

The results of Pb (II) removal efficiency from all 18 experimental runs designed by the FFD were summarized in Table 2. The removal efficiency was calculated based on effect values and regression coefficients (Table 3) using the least square of error technique (2).

$$Y = \beta_0 + \beta_1 X_1 + \beta_2 X_2 + \beta_3 X_3 + \beta_{1\,2} X_1 + \beta_{1\,3} X_1 X_3 + \beta_{2\,3} X_2 X_3 \pm \varepsilon, \quad (2)$$

where Y is the response (removal percentage of Pb (II)); β are the constant coefficients; X is the coded independent variable (X_1, X_2 and X_3 were corresponding coded variables of adsorbents, initial solution pH and adsorption time (min), respectively); and ε is the experimental error.

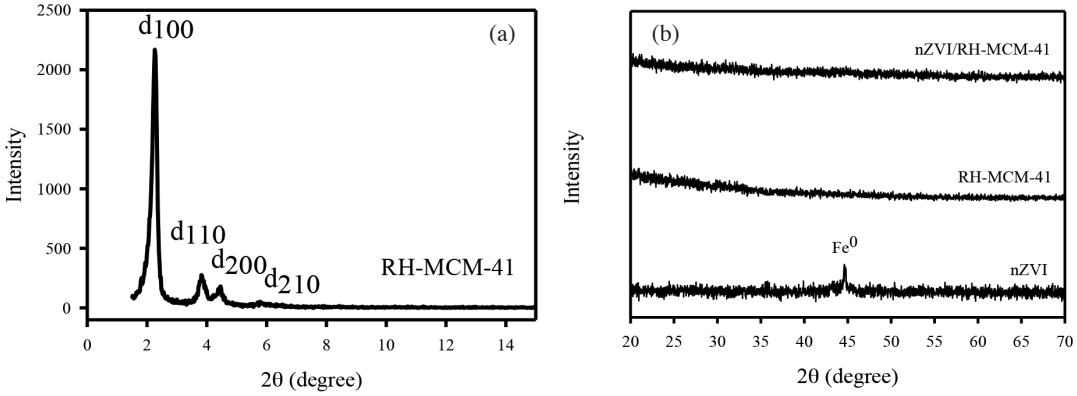

FIGURE 1. XRD patterns of (a) RH-MCM-41, (b) nZVI, RH-MCM-41 and nZVI coupled with RH-MCM-41

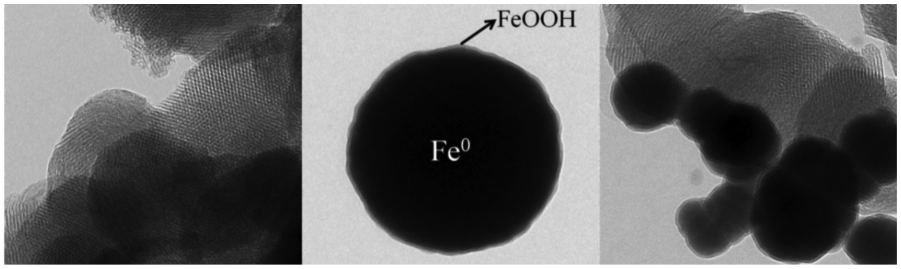

FIGURE 2. TEM results of (a) RH-MCM-41, (b) nZVI and (c) nZVI coupled with RH-MCM-41

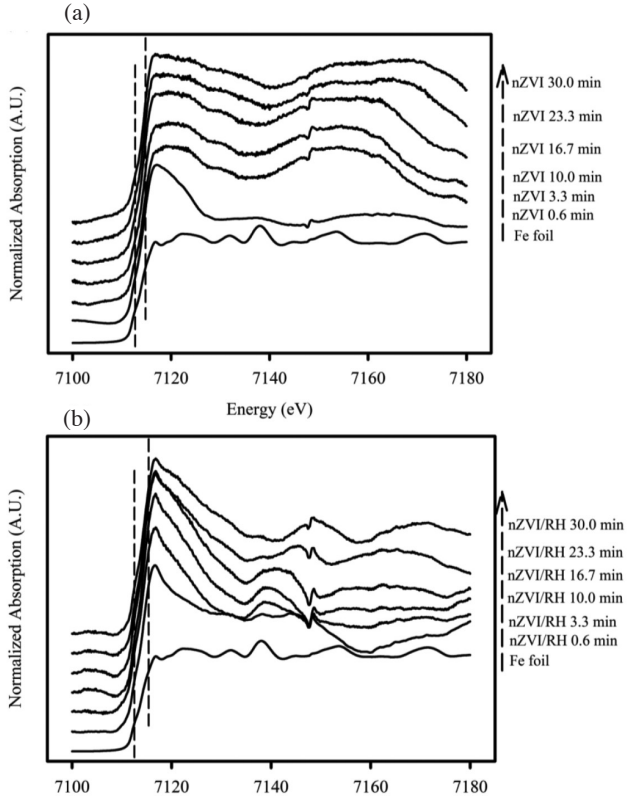

FIGURE 3. XANES spectrums of (a) nZVI and (b) nZVI coupled with RH-MCM-41

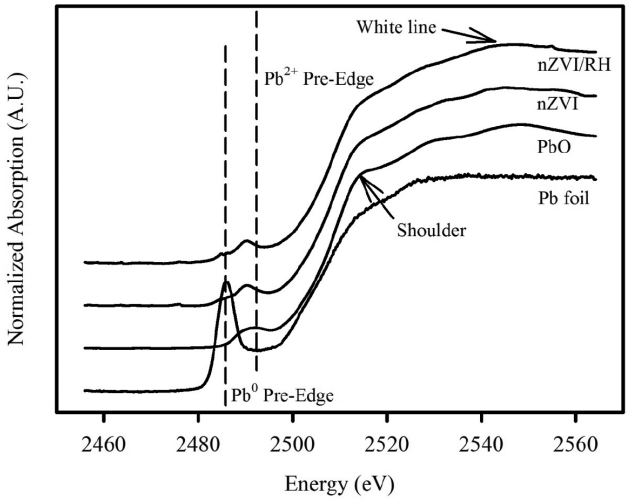

FIGURE 4. XANES spectrums of the adsorbent after adsorption process

As shown in Figure 5(a) to 5(d), significant experimental errors cannot be detected in all experimental runs. The diagnostic plots (Figure 5(a) to 5(d)) were used to confirm whether the predicted and experimental results of Pb (II) removal efficiency violated the assumptions of the analysis of variance (ANOVA). All plots, namely the linear normal probability plot (Figure 5(a)), the distribution of all results ranging from 10 to 80% (Figure 5(b)), the normal distribution of all data (Figure 5(c)) and the scattering of standard residuals to the observation order (Figure 5(d)), strongly guaranteed the accuracy and reliability of all results obtained from adsorption experiments. The results obtained were in good agreement with previous research results reported by Suwannaruang et al. (2015) and Wantala et al. (2015, 2012b). In addition, Figure 6 confirmed that pH of the initial solution with the coefficient value of 22.81 was the most significant factors affecting Pb (II) removal efficiency.

An approximate function of Pb (II) removal efficiency based on the experimental results was evaluated using (3).

TABLE 2. Optimization of Pb (II) adsorption experiments

Run order	Variables			Yexp (%)	Ypred (%)
	X_1	X_2	X_3		
1	nZVI coupled with RH-MCM-41	6	5	67.86	67.58
2	nZVI coupled with RH-MCM-41	4.5	7	43.06	43.29
3	nZVI	4.5	3	59.88	60.19
4	nZVI coupled with RH-MCM-41	4.5	5	41.87	41.95
5	nZVI	6	3	55.02	54.56
6	nZVI coupled with RH-MCM-41	3	7	16.15	16.09
7	nZVI coupled with RH-MCM-41	3	5	15.11	15.29
8	nZVI coupled with RH-MCM-41	6	3	66.07	66.52
9	nZVI	3	7	16.72	16.77
10	nZVI	3	5	16.14	15.95
11	nZVI	4.5	7	62.02	61.79
12	nZVI	3	3	15.68	15.81
13	nZVI/RH-MCM-41	4.5	3	40.73	40.41
14	nZVI/RH-MCM-41	3	3	13.99	13.85
15	nZVI/RH-MCM-41	6	7	69.02	68.84
16	nZVI	6	7	55.43	55.60
17	nZVI	4.5	5	60.52	60.43
18	nZVI	6	5	54.05	54.32

TABLE 3. Effect values and estimated regression coefficients of Pb (II) adsorption

Variables	Effects	Coefficients
Constant		42.74
Adsorbents (X_1)	-2.40	-1.20
Initial pH (X_2)	45.61	22.81
Adsorption time (X_3)	1.84	0.92
Adsorbents*Initial pH (X_1X_2)	6.96	3.48
Adsorbents*Adsorption time (X_1X_3)	0.64	0.32
Initial pH*Adsorption time (X_2X_3)	0.02	0.01

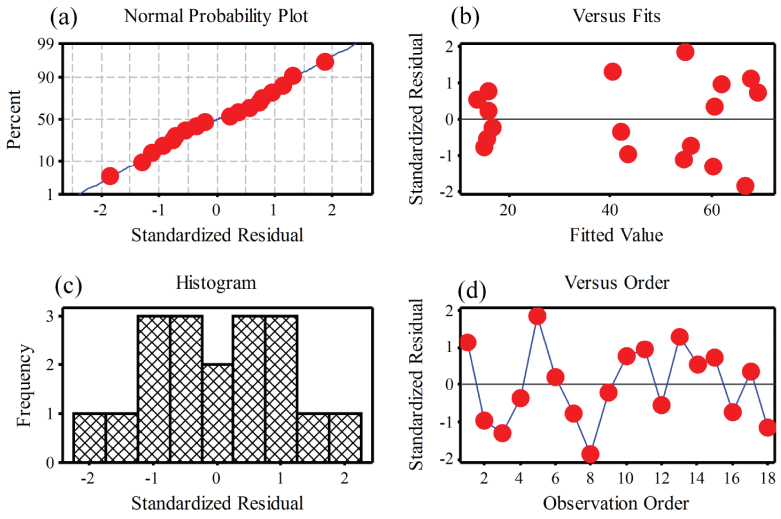

FIGURE 5. Diagnostic plots of the optimization study showing (a) normal probability plot, (b) versus fit, (c) histogram and (d) versus order

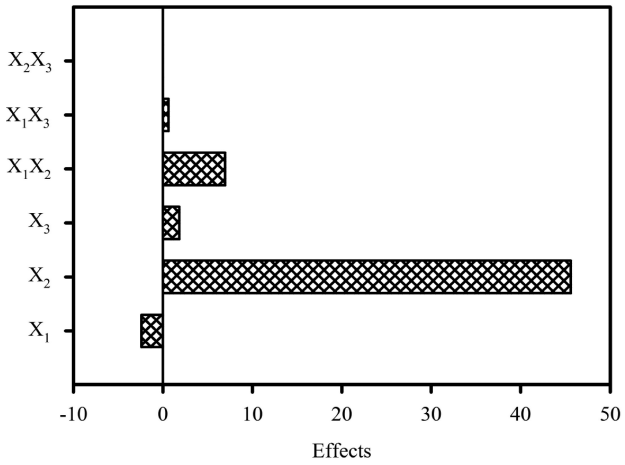

FIGURE 6. Factor effect levels affecting Pb (II) removal efficiency. Where X_1 is adsopbent, X_2 is initial pH and X_3 is adsorption time

The relationship between predicted values and experimental values shows good agreement with the regression coefficient close to 1. This result indicated a satisfactory approximation between the predicted model and the actual value.

$$Y(\%) = 42.74 - 1.20X_1 + 22.81X_2 + 0.92X_3 + 3.48X_1X_2 + 0.32X_1X_3 + 0.04X_2X_3 \quad (3)$$

where Y is predicted percentage of Pb (II) removal; X_1, X_2 and X_3 were corresponding coded variables of adsorbents; and initial solution pH and adsorption time (min), respectively.

Figure 7 shows the interaction plot of Pb (II) removal percentage. It proved that at the initial pH solution of 6, the removal of Pb (II) was higher than at the pH of 3. This might be caused by the lower number of hydronium ions (H^+) in the solution at pH of 6. When the initial pH of the solution was 3, the presence of a high number of H^+ may cover the surface of the adsorbents. As a result, H^+ may retard the adsorption of Pb (II) ions. In addition, a lower adsorption capacity of Pb (II) was also found at pH3. Concerning the removal efficiency of different adsorbents, it was found that nZVI coupled with RH-MCM-41 had a slightly higher adsorption capacity than nZVI due to the higher number of hydroxide surface sites on RH-MCM-41,which could facilitate Pb (II) adsorption. Another reason is that, for RH-MCM-41, the ferrous oxide (Fe^{2+}), ferric oxide (Fe^{3+}) and Pb^{2+} did not cover the nZVI and instead they were adsorbed on RH-MCM-41. Thus, RH-MCM-41 could enhanced the efficiency of Pb (II) removal by nZVI. Unlike pH and types of adsorbent, adsorption time was found to be an insignificant variable for Pb (II) removal.

The interaction effects of each variable including adsorbents, initial pH and adsorption time showed that the effects between adsorbents-adsorption time and initial pH-adsorption time were parallel, which is indicated that there is no interaction between these variables. On the other hand, the interaction plots between adsorbents and initial pH indicated a positive interaction between these two variables. In addition, enhanced Pb (II) adsorption capacity was found when RH-MCM-41 was used. This could have been resulted from the pH at the point of zero charge (pzc) on RH-MCM-41 surface, which was about 2 (Artkla et al. 2009). When the pH of the solution was 6, higher than the pzc, the surfaces of RH-MCM-41 become negative. As a result, more amounts of Pb (II) ions were adsorbed on the RH-MCM-41 and higher adsorption capacity was determined. The results obtained at the point of pH lower than the pzc were well matched to the finding above. The adsorption capacity of Pb (II) was low when the pH of solution was 3. This can be caused by the repulsiton between Pb (II) ions and the RH-MCM-41 surface with positive charges. The adsorption percentages of RH-MCM-41 and nZVI at the same initial pH of 6, were about 5 and 55, respectively. In contrast to the percentage of Pb (II) removal efficiency of nZVI coupled with RH-MCM-41 with the mass ratio 5 was almost 100. Thus, it can be concluded that high efficiency of Pb (II) adsorption can be enhanced by using the synergistic effects of nZVI and RH-MCM-41.

EQUILIBRIUM ADSORPTION ISOTHERM AND KINETIC ADSORPTION MODEL

The equilibrium isotherm of Pb (II) removal was determined using Langmuir (4) and Freundlich (5) isotherms, respectively:

$$\frac{C_e}{q_e} = \frac{1}{K_L q_m} + \frac{C_e}{q_m}. \quad (4)$$

$$\log q_e = \log K_F + \left(\frac{1}{n}\right)\log C_e, \quad (5)$$

where C_e is Pb (II) concentration in solution at equilibrium (ppm); q_e and q_m are the equilibrium and maximum adsorption capacity of Pb (II) (mg/g); respectively; and K_L and K_F are the constants of Langmuir and Freundlich isotherms, respectively.

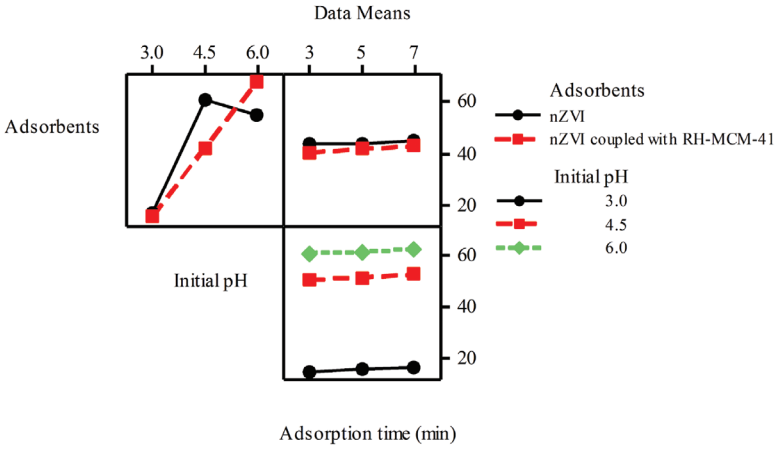

FIGURE 7. Interaction plots of Pb (II) removal percentage

The sorption energies were studied using Temkin (6) and Dubinin-Radushkevich (8) isotherms, respectively. Temkin isotherm:

$$q_e \beta \ln K_T + \beta \ln C_e. \quad (6)$$

$$\beta = \frac{RT}{b}, \quad (7)$$

where β is Temkin isotherm constant (mol^2/kJ^2); b is Temkin sorption energy (kJ/mol); R is gas constant; and K_T is Temkin equilibrium constant. The Temkin sorption energy was calculated using (7). The sorption energy less than 20 kJ/mol indicates physical adsorption.

Dubinin-Radushkevich isotherm:

$$\ln q_e = \ln q_d - \beta\varepsilon^2. \quad (8)$$

$$\varepsilon = RT \ln\left[1+\frac{1}{C_e}\right]. \quad (9)$$

$$E = \frac{1}{\sqrt{2\beta}}, \quad (10)$$

where β is Dubinin-Radushkevich isotherm constant; ε is Polanyi potential (9); and E is Dubinin-Radushkevich sorption energy (kJ/mol) (10). The sorption energies of less than 8 and 8-16 kJ/mol indicate physical adsorption and chemical adsorption, respectively.

Figure 8(a) and 8(b) shows the plots of experimental data regarding Langmuir and Freundlich isotherms. The fitted constants for the Langmuir and Freundlich isotherms along with the regression coefficients (R^2) are summarized in Table 4(a). The results were well-fitted with the Langmuir isotherm (R^2 = 0.98). This indicated that the Pb (II) adsorption on nZVI coupled with RH-MCM-41 is a monolayer adsorption. The adsorption was found to be specific on the OH-group of nZVI coupled with RH-MCM-41 surface. The maximum adsorption capacity was equal to 233 mg/g at the equilibrium time of 7 min. Moreover, the dimensionless constant separation factor (R_L) was calculated using (11). The value of R_L can be used to indicate the type of isotherm as unfavorable (R_L>1), linear (R_L = 1), favorable (0<R_L<1) or irreversible (R_L= 0) (Dada et al. 2012; Sun et al. 2013; Xu et al. 2012). The R_L values found in this study pointed out that Pb (II) adsorption on nZVI coupled with RH-MCM-41 is a favorable adsorption (R_L=0.0004-0.0009). In case of high initial concentration, R_L values close to 0, indicating an irreversible adsorption, was obtained. Moreover, the Temkin and Dubinin-Radushkevich isotherms were depicted in Figure 8(c) and 8(d), respectively. The sorption energy was calculated using (7) and (10). Temkin and Dubinin-Radushkevich sorption energies were about 0.073 and 5 kJ/mol, respectively. Therefore, it can be concluded that Pb (II) adsorption on nZVI coupled with RH-MCM-41 is a physical adsorption and there is no chemical reaction between Pb (II) and nZVI coupled with RH-MCM-41 surface. However, regarding to XANE results, the sorption of Pb (II) was found on the OH-group of nZVI coupled with the RH-MCM-41 surface.

$$R_L = \frac{1}{1+K_L C_0}, \quad (11)$$

where R_L is dimensionless constant separation factor; C_0 is initial concentration of Pb (II); and K_L is Langmuir isotherm constant, respectively.

The kinetic adsorptions were determined by the pseudo-first order (12), pseudo-second order (13), intrapaticle diffusion (14) and Langmuir- Hinshelwood (LH) (15) models.

$$\ln (q_e - q_t) = \ln q_e - k_f t, \quad (12)$$

where $q_e$bis equilibrium adsorption capacity (mg/g); q_t is adsorption capacity at time t (mg/g); and k_f is pseudo-first order rate constant of adsorption (1/min), which can be calculated from the slope of a plot of ln ($q_e - q_t$) versus t.

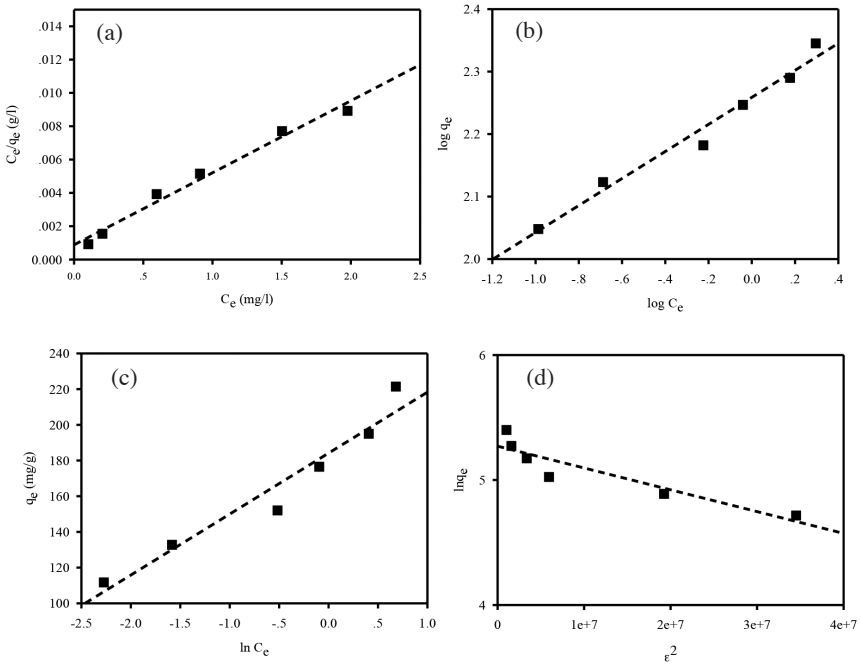

FIGURE 8. Results of (a) Langmuir, (b) Freundlich, (c) Temkin and (d) Dubinin-Radushkevich (D-R) isotherms

$$\frac{t}{q_t} = \frac{1}{k_2 q_2^2} + \frac{1}{q_2} t \tag{13}$$

where q_2 is maximum adsorption capacity of pseudo-second order (mg/g); q_t is adsorption capacity at time t (mg/g); and k_2 is pseudo-second order rate constant of adsorption (g/mg.min) which can be calculated from the intercept of a plot of $\frac{t}{q_t}$ versus t.

$$q_t = k_i t^{1/2} + C, \tag{14}$$

where k_i is the intraparticle diffusion rate constant (mg/g. $min^{1/2}$); which can be calculated from the slope of a plot of q_t versus $t^{1/7}$ to get the intercept C.

$$\frac{1}{r_0} = \frac{1}{K_{ad} k_r C_0} + \frac{1}{k^r}, \tag{15}$$

where r_0 and C_0 are initial reaction rate and initial concentration of Pb (II) respectively; K_{ad} is adsorption coefficient and K_r is reaction rate constant; and the slope and intercept of the plot between $\frac{1}{r_0}$ versus $\frac{1}{C_0}$ can be used to compute K_{ad} and k_r, respectively.

Figure 9(a) to 9(c) and Table 4(b) shows the results of kinetic adsorptions. These results of Pb (II) removal fitted well with the pseudo-second order model with R^2 close to 1. It can be furher implied that the adsorption process is the rate controlling step of Pb (II) removal using nZVI coupled with RH-MCM-41. In addition, it can be concluded that Pb (II) is especially adsorbed on the surface of nZVI coupled with the RH-MCM-41. The adsorption capacity of pseudo-second order, therefore, can be increased with the increase in the Pb (II) initial concentration. With the initial concentration of 250 to 500 ppm, the adsorption capacity was found to be ranged from 112 to 221 mg/g. Thus, the results obtained clearly confirmed that nZVI coupled with RH-MCM-41 can be used as an adsorbent of high Pb (II) concentrations. There are several pathways which can be included in the specific adsorption mechanisms of Pb (II). One of the pathways is the reduction of Pb^{2+} to Pb^0 due to the standard electrode potential of Pb^{2+}/Pb^0 (-0.13V) is more positive than Fe^{2+}/Fe^0 (-0.44V). Thus, Pb^{2+} can be reduced to Pb^0 by Fe^{2+} (Li & Zhang 2007; Pojananukij et al. 2016). Another pathway is Pb (II) adsorption on the OH-group of nZVI or RH-MCM-41 surface.

The adsorption on surface of adsorbent can be confirmed using the Langmuir- Hinshelwood (LH) model (Kumar et al. 2008). The initial rates (Figure 9(d)) were calculated using (15). The values of K_{ad} and k_r were 0.0002 L/mg and 5000 mg/L.min, respectively. Thus, it can be implied that reduction reaction and adsorption on FeOOH are significant pathways of Pb (II) removal by nZVI coupled RH-MCM-41.

For the intraparticle diffusion model, the correlation coefficients were lower than those coefficients determined by the pseudo-second order model. Since the plot did not pass through the origin, it can be referred that intraparticle diffusion is not a rate-limiting step of Pb (II) adsorption. However, the straight plot (Figure 9(c)) indicates that Pb (II) adsorption may follow the intraparticle diffusion model for up to 7 min. Therefore, it can be concluded that there is a diffusion of Pb^0 into the RH-MCM-41 porous surface after the reduction process.

TABLE 4. Isotherm constants of Pb (II) removal

(a) Equilibrium adsorption isotherms

Isotherm model	Langmuir	Freundlich	Temkin	Dubinin-Radushkevich (D-R)
	q_m = 233 mg/g K_L = 4.78 l/mg	n = 4.62 K_F = 181.45 l/mg	b = 0.073 kJ/mol K_T = 219.35	q_d = 194 mg/g E = 5.00 kJ/mol
R^2	0.98	0.97	0.94	0.85

(b) Kinetic adsorption isotherms

Concentrations (ppm)	q_e (mg/g)	Pseudo-first order		Pseudo-second order		Intraparticle diffusion	
		k_f (min^{-1})	R^2	k_2 (g/mg.min)	R^2	k_i ($mg.min^{0.5}/g$)	R^2
250	112	0.510	0.60	0.158	0.99	1.977	0.81
300	132	0.653	0.81	0.060	0.99	6.233	0.97
350	152	0.685	0.80	0.060	1.00	7.771	0.88
400	174	0.786	0.72	0.063	1.00	8.296	0.87
450	195	0.745	0.68	0.087	1.00	4.898	0.88
500	221	0.729	0.83	0.039	0.99	14.135	0.80

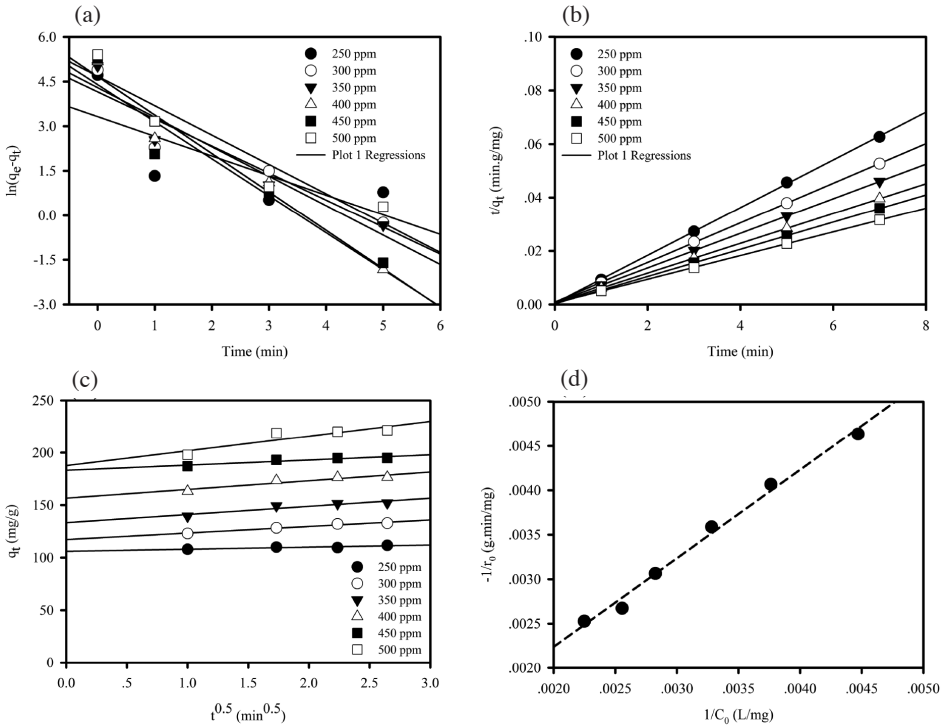

FIGURE 9. Results of kinetic adsorptions determined by (a) Pseudo-first order, (b) Pseudo-second order, (c) Intraparticle diffusion and (d) the Langmuir- Hinshelwood (LH) plots

According to the results reported by Pojananukij et al. (2016), mechanisms of Pb (II) adsorption on zero-valent iron coated on diatomite (NZI-D) can be classified into 2 steps including Pb (II) reduction and reaction of Pb with iron oxide and hydroxide. The reduction of Pb^{2+} to Pb^0, the first step, can be explained by the standard reduction potential of Pb^{2+}/Pb^0 (-0.1263 V) which is higher than that of Fe^{2+}/Fe^0 (-0.4402 V). The other step is the reaction between iron oxide/hydroxide and Pb (II) to form FeOPbOH, PbO-Fe, PbO_2-Fe_2O_3, and PbO-FeOOH on surface of zero-valent irons. Pojananukij et al. (2016) also reported the adsorption of Pb (II) on Si–OH and Si–O sites to form the PbO_2–Si and PbO–Si. Thus, regarding XANES, adsorption results of this present study and results reported by Pojananukij et al. (2016), there were 4 possible pathways for Pb (II) removal by nZVI coupled with RH-MCM-41 (Figure 10). They were: the reduction process of Pb^{2+} to Pb^0, the adsorption of Pb (II) on FeOOH, the adsorption of Pb (II) on RH-MCM-41 surface and the complex reaction between Fe and Pb ions.

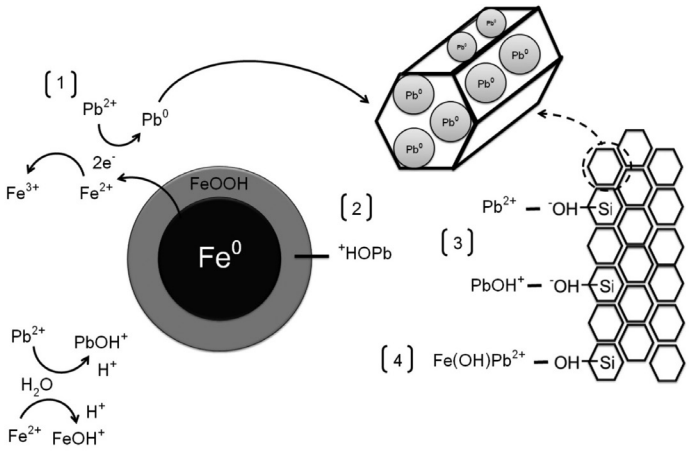

FIGURE 10. Model of Pb (II) removal mechanisms by nZVI coupled with RH-MCM-41

TABLE 5. Adsorption capacity and equilibrium time of different adsorbents

Adsorbent	Concentration (ppm)	Model	q_{max} (mg/g)	T_E (min)	Reference
Chitosan-coated sand (CCS)	100-2000	L	12.32	240	(Wan et al. 2010)
Apple Pomace	10-200	L	16.39	80	(Chand & Pakade 2013)
Manganoxide minerals	250	L	98	120	(Sonmezay et al. 2012)
Rice husk ash	40	L	12.61	300	(Feng et al. 2004)
Rice husk ask	10-300	L	91.74	60	(Naiya et al. 2009)
Chitosan bead	50-200	L	73.52	30	(Lu et al. 2013)
Cow bone activated carbon	25-400	L	47.62	360	(Cechinel et al. 2014)
Valonia tannin resin (VTR)	20-100	L	138.9	60	(Şengil & Özacar 2009)
Orange peel	200	L	113.5	120	(Feng & Guo 2012)
Modified orange peel	200	L	209.8	120	(Feng & Guo 2012)
Kaolinite clay	100	L	2.35	60	(Jiang et al. 2010)
K-nZVI	50-1000	-	440.5	60	(Zhang et al. 2011)
nZVI coupled with RH-MCM-41	250-500	L	233	7	This study
nZVI coupled with RH-MCM-41	500	2nd	222	7	This study

Note : T_E is the adsorption equilibrium time

The comparison of adsorption capacity and equilibrium time of different adsorbents are summarized in Table 5. The results indicated that though the highest maximum adsorption capacity could not be observed in all adsorbents, the shortest adsorption equilibrium time was obtained.

CONCLUSION

nZVI coupled with RH-MCM-41 can be used for Pb (II) adsorption at a neutral condition. When comparing nZVI and nZVI coupled with RH-MCM-41, the latter shows a slightly higher adsorption capacity because RH-MCM-41 contains a higher amount of hydroxide surface sites, which could facilitate the adsorption of Pb (II). The other reason, for Pb (II) removal by RH-MCM-41, can be attributed to the uncovering of ferrous oxide (Fe^{2+}), ferric oxide (Fe^{3+}) and Pb^{2+} on nZVI surface. Instead, they were adsorbed on the surface of RH-MCM-41. Thus, RH-MCM-41 can enhance the efficiency of nZVI. The removal percentage of Pb (II) increases with increasing initial pH of the solution. The H^+ at the acidic condition may prevent Pb (II) hydroxide to be adsorbed on nZVI coupled with RH-MCM-41. The removal mechanism of Pb (II) which was well fitted with the Langmuir isotherm indicated that Pb (II) adsorption is a monolayer adsorption. The maximum adsorption capacity was approximately 233 mg/g. The sorption energies calculated by the Temkin and Dubinin-Radushkevich (D-R) isotherm were 0.073 and 5.00 kJ/mol, respectively. Therefore, the adsorption of Pb (II) on nZVI coupled with RH-MCM-41 is a physical adsorption. For kinetic studies, Pb (II) removal can be explained by the pseudo-second order model. The adsorption process was found to be a rate limiting step for Pb (II) removal. The reduction reaction, indicated by the LH, is a significant pathway for Pb (II) removal. The mechanisms of Pb (II) removal include reduction process, adsorption on FeOOH, adsorption on RH-MCM-41 and complex reaction between Fe and Pb ions.

ACKNOWLEDGMENTS

This study was financially supported by the Faculty of Engineering, Khon Kaen University, Thailand and the International Environmental research Center (IEAEC), Gwangju Institute of Science and Technology, Republic of Korea. The authors would like to acknowledge the Synchrotron Light Research Institute (Public Organization) Thailand for the courtesy on XANES measurement (BL5.2: SUT-NANOTEC-SLRI XAS Beamline and BL2.2).

REFERENCES

Ahn, S.C., Oh, S.Y. & Cha, D.K. 2008. Enhanced reduction of nitrate by zero-valent iron at elevated temperatures. *Journal of Hazardous Materials* 156(1-3): 17-22.

Artkla, S., Kim, W., Choi, W. & Wittayakun, J. 2009. Highly enhanced photocatalytic degradation of tetramethylammonium on the hybrid catalyst of titania and MCM-41 obtained from rice husk silica. *Applied Catalysis B: Environmental* 91(1-2): 157-164.

ATSDR. 2007. Toxicological Profile: Lead. http://www.atsdr.cdc.gov/toxprofiles/tp.asp?id=96&tid=22. Accessed on 7 July 2015.

Babel, S. & Kurniawan, T.A. 2003. Low-cost adsorbents for heavy metals uptake from contaminated water: A review. *Journal of Hazardous Materials* 97(1-3): 219-243.

Bhatnagar, A., Vilar, V.J.P., Botelho, C.M.S. & Boaventura, R.A.R. 2011. A review of the use of red mud as adsorbent for the removal of toxic pollutants from water and wastewater. *Environmental Technology* 32(3): 231-249.

Boparai, H.K., Joseph, M. & O'Carroll, D.M. 2013. Cadmium (Cd^{2+}) removal by nano zerovalent iron: surface analysis, effects of solution chemistry and surface complexation modeling. *Environmental Science and Pollution Research* 20(9): 6210-6221.

Case Studies in Environmental Medicine (CSEM): Lead toxicity. 2010. U.S. Department of Human Services, Public Health Service, Agency for Toxic Substance and Disease Registry (ATSDR).

Cechinel, M.A.P., Ulson de Souza, S.M.A.G. & Ulson de Souza, A.A. 2014. Study of lead (II) adsorption onto activated carbon originating from cow bone. *Journal of Cleaner Production* 65: 342-349.

Centers for Disease Control and Prevention. 2005. Preventing Lead Poisoning in Young Children. Atlanta: the Centers for Disease Control and Prevention.

Chand, P. & Pakade, Y.B. 2013. Removal of Pb from water by adsorption on apple pomace: equilibrium, kinetics, and thermodynamics studies. *Journal of Chemistry* 2013: e164575.

Dada, A.O., Olalekan, A.P., Olatunya, A.M. & DADA, O. 2012. Langmuir, Freundlich, Temkin and Dubinin-Radushkevich isotherms studies of equilibrium sorption of Zn^{2+} unto phosphoric acid modified rice husk. *IOSR Journal of Applied Chemistry* 3(1): 38-45.

Feng, N. & Guo, X. 2012. Characterization of adsorptive capacity and mechanisms on adsorption of copper, lead and zinc by modified orange peel. *Transactions of Nonferrous Metals Society of China* 22(5): 1224-1231.

Feng, Q., Lin, Q., Gong, F., Sugita, S. & Shoya, M. 2004. Adsorption of lead and mercury by rice husk ash. *Journal of Colloid and Interface Science* 278(1): 1-8.

Hwang, Y.H., Kim, D.G. & Shin, H.S. 2011. Mechanism study of nitrate reduction by nano zero valent iron. *Journal of Hazardous Materials* 185(2-3): 1513-1521.

Jiang, M., Jin, X., Lu, X.Q. & Chen, Z. 2010. Adsorption of Pb(II), Cd(II), Ni(II) and Cu(II) onto natural kaolinite clay. *Desalination* 252(1-3): 33-39.

Kim, S.A., Kamala-Kannan, S., Lee, K.J., Park, Y.J., Shea, P.J. & Lee, W.H. 2013. Removal of Pb(II) from aqueous solution by a zeolite–nanoscale zero-valent iron composite. *Chemical Engineering Journal* 217: 54-60.

Krasae, N., Wantala, K., Tantriratna, P. & Grisdanurak, N. 2014. Removal of nitrate by bimetallic copper-nanoscale zero-valent iron. *Applied Environmental Research* 36(2): 15-23.

Kržišnik, N., Mladenovič, A., Škapin, A.S., Škrlep, L., Ščančar, J. & Milačič, R. 2014. Nanoscale zero-valent iron for the removal of Zn^{2+}, Zn(II)–EDTA and Zn(II)–citrate from aqueous solutions. *Science of the Total Environment* 476-477: 20-28.

Kumar, K.V., Porkodi, K. & Rocha, F. 2008. Langmuir–Hinshelwood kinetics - A theoretical study. *Catalysis Communications* 9(1): 82-84.

Liang, W., Dai, C., Zhou, X. & Zhang, Y. 2014. Application of zero-valent iron nanoparticles for the removal of aqueous zinc ions under various experimental conditions. *PLoS ONE* 9(1): e85686.

Li, X. & Zhang, W. 2007. Sequestration of metal cations with zerovalent iron nanoparticles - a study with high resolution x-ray photoelectron spectroscopy (HR-XPS). *The Journal of Physical Chemistry C* 111(19): 6939-6946.

Lu, Y., He, J. & Luo, G. 2013. An improved synthesis of chitosan bead for Pb(II) adsorption. *Chemical Engineering Journal* 226: 271-278.

Melo, R.A.A., Giotto, M.V., Rocha, J. & Urquieta-González, E.A. 1999. MCM-41 ordered mesoporous molecular sieves synthesis and characterization. *Materials Research* 2(3): 173-179.

Naiya, T.K., Bhattacharya, A.K., Mandal, S. & Das, S.K. 2009. The sorption of lead(II) ions on rice husk ash. *Journal of Hazardous Materials* 163(2-3): 1254-1264.

Notification of Ministry of Industry Thailand, No 12, B.E. 2542. 1999. Royal Government Gazette. 112 Part 29D (under the Groundwater Act, B.E. 2520 (1977)).

Occupational Knowledge International. 2010, 2012. Summary of mass lead poisoning incidents. Occupational Knowledge International (OK International).

Oh, Y.J., Song, H., Shin, W.S., Choi, S.J. & Kim, Y.H. 2007. Effect of amorphous silica and silica sand on removal of chromium(VI) by zero-valent iron. *Chemosphere* 66(5): 858-865.

Onweremadu, E.U. 2008. Physico-chemical characterization of a farmland affected by wastewater in relation to heavy metals. *Journal of Zhejiang University SCIENCE A* 9(3): 366-372.

Pojananukij, N., Wantala, K., Neramittapapong, S. & Neramittapapong, A. 2016. Equilibrium, kinetics, and mechanism of lead adsorption using zero-valent iron coated on diatomite. *Desalination and Water Treatment* 57(39): 18475-18489.

Ponder, S.M., Darab, J.G. & Mallouk, T.E. 2000. Remediation of Cr(VI) and Pb(II) aqueous solutions using supported, nanoscale zero-valent iron. *Environmental Science & Technology* 34(12): 2564-2569.

Şengil, İ. A. & Özacar, M. 2009. Competitive biosorption of Pb^{2+}, Cu^{2+} and Zn^{2+} ions from aqueous solutions onto valonia tannin resin. *Journal of Hazardous Materials* 166(2-3): 1488-1494.

Sonmezay, A., Öncel, M.S. & Bektas, N. 2012. Adsorption of lead and cadmium ions from aqueous solutions using manganoxide minerals. *Transactions of Nonferrous Metals Society of China* 22(12): 3131-3139.

Sun, C.J., Sun, L.Z. & Sun, X.X. 2013. Graphical evaluation of the favorability of adsorption processes by using conditional Langmuir constant. *Industrial & Engineering Chemistry Research* 52(39): 14251-14260.

Sun, Y.P., Li, X., Cao, J., Zhang, W. & Wang, H.P. 2006. Characterization of zero-valent iron nanoparticles. *Advances in Colloid and Interface Science* 120(1-3): 47-56.

Suwannaruang, T., Rivera, K.K.P., Neramittagapong, A. & Wantala, K. 2015. Effects of hydrothermal temperature and time on uncalcined TiO2 synthesis for reactive red 120 photocatalytic degradation. *Surface and Coatings Technology* 271: 192-200.

Tanboonchuy, V., Hsu, J.C., Grisdanurak, N. & Liao, C.H. 2011. Gas-bubbled nano zero-valent iron process for high concentration arsenate removal. *Journal of Hazardous Materials* 186(2-3): 2123-2128.

Wan, M.W., Kan, C.C., Rogel, B.D. & Dalida, M.L.P. 2010. Adsorption of copper (II) and lead (II) ions from aqueous solution on chitosan-coated sand. *Carbohydrate Polymers* 80(3): 891-899.

Wantala, K., Khamjumphol, C., Thananukool, N. & Neramittagapong, A. 2015. Degradation of reactive Red 3 by heterogeneous Fenton-like process over iron-containing RH-MCM-41 assisted by UV irradiation. *Desalination and Water Treatment* 54(3): 699-706.

Wantala, K., Sthiannopkao, S., Srinameb, B., Grisdanurak, N., Kim, K.W. & Han, S. 2012a. Arsenic adsorption by Fe loaded on RH-MCM-41 synthesized from rice husk silica. *Journal of Environmental Engineering* 138(1): 119-128.

Wantala, K., Khongkasem, E., Khlongkarnpanich, N., Sthiannopkao, S. & Kim, K.W. 2012b. Optimization of As(V) adsorption on Fe-RH-MCM-41-immobilized GAC using Box-Behnken design: Effects of pH, loadings, and initial concentrations. *Applied Geochemistry* 27(5): 1027-1034.

Wantala, K., Sthiannopkao, S., Srinameb, B., Grisdanurak, N. & Kim, K.W. 2010. Synthesis and characterization of Fe-MCM-41 from rice husk silica by hydrothermal technique for arsenate adsorption. *Environmental Geochemistry and Health* 32(4): 261-266.

WHO|WHO Guidelines for drinking-water quality. 2011. *WHO*. http://www.who.int/water_sanitation_health/dwq/guidelines/en/. Accessed on 7 July 2015.

Xu, P., Zeng, G.M., Huang, D.L., Lai, C., Zhao, M.H., Wei, Z., Li, N.J., Huang, C. & Xie, G.X. 2012. Adsorption of Pb(II) by iron oxide nanoparticles immobilized Phanerochaete chrysosporium: equilibrium, kinetic, thermodynamic and mechanisms analysis. *Chemical Engineering Journal* 203: 423-431.

Yan, W., Herzing, A.A., Kiely, C.J. & Zhang, W. 2010. Nanoscale zero-valent iron (nZVI): aspects of the core-shell structure and reactions with inorganic species in water. *Journal of Contaminant Hydrology* 118(3-4): 96-104.

Zhang, W. 2003. Nanoscale iron particles for environmental remediation: an overview. *Journal of Nanoparticle Research* 5(3-4): 323-332.

Zhang, X., Lin, S., Chen, Z., Megharaj, M. & Naidu, R. 2011. Kaolinite-supported nanoscale zero-valent iron for removal of Pb^{2+} from aqueous solution: Reactivity, characterization and mechanism. *Water Research* 45(11): 3481-3488.

Zhang, X., Lin, S., Lu, X.Q. & Chen, Z. 2010. Removal of Pb(II) from water using synthesized kaolin supported nanoscale zero-valent iron. *Chemical Engineering Journal* 163(3): 243-248.

Zhang, Y., Li, Y., Dai, C., Zhou, X. & Zhang, W. 2014. Sequestration of Cd(II) with nanoscale zero-valent iron (nZVI): Characterization and test in a two-stage system. *Chemical Engineering Journal* 244: 218-226.

Zhang, Y., Su, Y., Zhou, X., Dai, C. & Keller, A.A. 2013. A new insight on the core-shell structure of zerovalent iron nanoparticles and its application for Pb(II) sequestration. *Journal of Hazardous Materials* 263(Part 2): 685-693.

Chatkamol Kaewbuddee & Kitirote Wantala*
Department of Chemical Engineering
Faculty of Engineering
Khon Kaen University
Khon Kaen 40002
Thailand

Chatkamol Kaewbuddee & Kitirote Wantala*
Chemical Kinetics and Applied Catalysis Laboratory (CKCL)
Faculty of Engineering, Khon Kaen University
Khon Kaen 40002
Thailand

Chatkamol Kaewbuddee & Kitirote Wantala*
Research Center for Environmental and Hazardous Substance Management (EHSM)
Faculty of Engineering, Khon Kaen University
Khon Kaen 40002
Thailand

Penradee Chanpiwat
Environmental Research Institute
Chulalongkorn University
Bangkok 10330
Thailand

Pinit Kidkhunthod
Synchrotron Light Research Institute
Nakhon Ratchasima, 30000
Thailand

*Corresponding author; email: kitirote@kku.ac.th

Received: 02 November 2015
Accessed: 23 January 2016